Chemical Engineering Science 325 (2026) 123447

Contents lists available at ScienceDirect

Chemical Engineering Science

journal homepage: www.elsevier.com/locate/ces

Parameter estimation of a size-exclusion simulated moving bed for protein purification via meta-heuristic methods with estimability analysis and uncertainty evaluation

Guilherme C. Amaral [a], Albertina G. Rios [a], Alírio E. Rodrigues [a], Ana M. Ribeiro [a], Diogo Rodrigues [a], Idelfonso B.R. Nogueira [b], Alexandre F.P. Ferreira [a,*]

[a] LSRE-LCM, ALiCE, Faculty of Engineering, University of Porto, Rua Dr. Roberto Frias, 4200-465 Porto, Portugal
[b] Chemical Engineering Department, Norwegian University of Science and Technology, Sem Sælandsvei 4, Kjemiblokk 5, Trondheim 793101, Norway

ARTICLE INFO

Keywords:
Adsorption
SMB
Optimization
Parameter estimation
PSO

ABSTRACT

This study aims to enhance the modelling of myoglobin (Mb) and bovine serum albumin (BSA) separation in size-exclusion gel systems by leveraging experimental data and computational methods. The objective is to estimate the parameters of a mathematical model that accurately represents this separation process. To achieve this, optimization problems with adequate objective functions are solved via Particle Swarm Optimization (PSO), which has been shown to be more efficient than comparable deterministic methods Comprehensive estimability and uncertainty analyses were also conducted to thoroughly assess the model's reliability and accuracy. The initial phase of the study involved estimating parameters for a fixed bed system. During this phase, it was discerned through estimability analysis that the mass transfer coefficient parameters, denoted as k_h, had minimal impact on the model's outputs, leading to their exclusion from subsequent estimations. The focus then shifted to refining the model parameters to simultaneously fit both the fixed bed and Simulated Moving Bed (SMB) experimental data. The comparative analysis between these parameters and the fixed bed parameters highlighted notable differences, particularly in the axial dispersion parameter (D_{ax}) and the BSA size exclusion constant ($K_{SEC,BSA}$). An uncertainty evaluation was successfully executed after completing this study, providing confidence intervals for each parameter, and propagating the uncertainty to the prediction of the developed model. This comprehensive approach ensures a more accurate and reliable understanding of the separation dynamics in size-exclusion gel processes for Mb and BSA.

1. Introduction

Proteins are found in every living organism and play a crucial role in the biochemical reactions occurring within biological systems. Proteins comprise 20 unique amino acids and exhibit a wide range of structural diversity and complexity. Their function heavily depends on these factors since the three-dimensional structure of the macromolecule and the sequence of amino acids collectively determine the characteristic properties of each protein (Whitford, 2013). Proteins exhibit numerous roles within the human body, contributing to cellular growth and tissue development, as well as in industrial applications, such as food supplements (Kumar, 2022), research, diagnostics, and therapeutic tools in the pharmaceutical sector (Hey et al., 2005), in membrane-based operations (Ryu, et al., 2019), and more. Hence, protein separation and purification processes are critical to facilitate the study and application of these essential molecules.

Protein separation usually encompasses various stages with distinct objectives. These stages can vary in number, but their purpose remains consistent, typically including recovery, concentration, purification, and product formulation (Nfor, 2008). Several different methodologies may be utilized to purify the proteins (Nfor, 2008; Smith, 2017; Saxena et al., 2009). Although membrane and electrochemical techniques may be employed, they rarely achieve the desired purities. Therefore, chromatography may also be used since this technique displays versatility and adaptability to the different properties of these nutrients, resulting in ample current use (Liu et al., 2020).

In chromatography, the sample is introduced into a column or a carrier containing a stationary phase. The mobile phase transports the

* Corresponding author.
E-mail addresses: up201806722@up.pt (G.C. Amaral), aferreir@fe.up.pt (A.F.P. Ferreira).

https://doi.org/10.1016/j.ces.2026.123447
Received 6 May 2025; Received in revised form 21 January 2026; Accepted 24 January 2026
Available online 25 January 2026
0009-2509/© 2026 The Authors. Published by Elsevier Ltd. This is an open access article under the CC BY license (http://creativecommons.org/licenses/by/4.0/).

sample through the equipment. Due to the varying affinities of the sample proteins to the stationary phase, they travel through the vessel at different velocities, resulting in different retention times. This difference enables the separation of the components (Lundanes et al., 2013). As the name implies, size-exclusion chromatography achieves separation due to the proteins' different dimensions. The smaller proteins will enter the gel's pores, increasing their retention time, while larger proteins rarely penetrate the orifices and will elute through the column without the solid phase's influence. Hence, the selectivity in this type of separation is dictated by the sieve dimensions of the gel, and no effective adsorption occurs (Hunt and Holding, 2013).

Since this type of chromatography has a relatively simple mechanism, it can be employed in an array of distinct equipment. Yet, some traditional column chromatography techniques are rather expensive. The Simulated Moving Bed (SMB) is an alternative to perform economical chromatography since the countercurrent movement emulated by the equipment yields high productivity and low mobile and stationary phase consumption, reducing costs (Houwing, 2003). An SMB unit is comprised of chromatographic columns in series, in a closed loop setup, where the inlet and outlet streams periodically shift in the direction of the fluid phase, simulating the countercurrent movement of the solid phase (Rodrigues, 2015).

Rigorous mathematical models help to understand phenomena in chromatographic processes. Four key components are usually required to model liquid-solid adsorption, depending on the case studied: bulk phase mass transport/transfer (convective and molecular diffusion), diffusion across the film to the adsorbent surface, intraparticle mass transfer (pore diffusion and surface diffusion), and adsorption/desorption equilibrium (Xu et al., 2013). Therefore, by solving a set of defined algebraic and partial differential equations, it is possible to gain insight into adsorption data and predict the behavior during separation and purification, reducing the need for excessive, costly, and time-consuming experiments (Xu et al., 2013).

Several methods may be employed to optimally estimate the parameters of these mathematical models that characterize the separation and purification processes. Although analytical methods are desirable, they often prove complex and impractical in engineering problems. Consequently, optimization problems are solved by deterministic or meta-heuristic methods. Deterministic methods guarantee a locally optimal solution upon convergence, but heavily rely on the initial guess (Pinto and Schwaab, 2007). Hence, they are effective for simpler engineering problems due to their quick convergence and accuracy. However, in complex scenarios such as nonconvex or large-scale problems, deterministic techniques may require a long time to converge or fail to do so. In such cases, meta-heuristic approaches are recommended due to their flexibility, as they rely less on initial guesses or conditions (Lin et al., 2012), and are capable of finding near-optimal solutions. This significantly reduces the time required to find close-to-optimal solutions to complex engineering problems and enables solving problems where exact/analytical or deterministic methods are unpracticable (Martí and Reinelt, 2022). Nonetheless, the computing power needed is much higher when compared to other approaches. Although this is manageable for simpler problems, as the complexity of the problem increases, the required computing power also escalates (Rao, 2019). For an SMB process, due to its cyclic and nonlinear nature, meta-heuristic methodologies may be preferred to ease computational effort and guarantee convergence. Moreover, a meta-heuristic method may be beneficial in the event that the selected algorithm converges into a local optimum, which would be detrimental if a deterministic method was instead used. There exists a plethora of different heuristic techniques ranging from swarm intelligence to evolutionary computation (Coelho and Sierakowski, 2008). Swarm intelligence is the tool employed in this work, particularly Particle Swarm Optimization (PSO), since it has been shown that PSO achieves similar results more efficiently than methods such as Genetic Algorithms or Simulated Annealing for similar case studies (Schwaab, 2005). PSO is a technique for continuous nonlinear function optimization, drawing inspiration from swarm behavior, evolutionary computation, and genetic algorithms. It uses a defined set of particles that search for the optimal solution using based on both individual memory and the swarm's collective knowledge (Kennedy and Eberhart, 1995).

In parameter estimation, complementary analyses are often needed to better characterize the results and validate the methodology employed. Local estimability analysis may use sensitivity matrices and their orthogonalization, to identify possible parameter correlations, quantify their influence, and simplify the optimization problem (Yao et al., 2003). Estimability methods assess the viability of estimating certain parameters based on the system input and output data. This is especially useful in complex problems, where parameter correlation often hinders successful estimation (Nogueira et al., 2016; Nogueira and Pontes, 2017). Additionally, to reduce measurement errors, incorporating uncertainty analysis is essential, thought it requires a comprehensive knowledge of all contributing factors (Iso and OIML, 1995). Monte Carlo simulations can aid in estimation and optimization problems by providing insight into model output and uncertainty (Kroese et al., 2014). It is also important to adjust measured data and estimated parameters to ensure consistency with conservation laws and other constraints, which may be violated due to the errors and variability. The general data reconciliation problem is typically addressed using weighted least-squares minimization of the error between the measurements and the model predictions subject to these constraints (Crowe, 1996).

In the existing literature, several studies have explored the use of PSO to perform parameter estimation for various distinct scenarios (Santos, 2021; Schwaab et al., 2008,; He et al., 2007; Gill et al., 2006; Ouyang et al., 2014; Sakthivel et al., 2010), so the use of this meta-heuristic method for the purpose of estimating parameters is well established in literature. In another hand, there are also studies focused on parameter estimation for SMB experiments which utilize different methodologies. Grosfils *et al.* employed a deterministic method based on quadratic approximation (Grosfils et al., 2010; Grosfils et al., 2007), while Bentley *et al.* utilized the SRQPD gPROMS solver, which is likewise deterministic in nature (Bentley et al., 2013). Deterministic methods remain the most prevalent type for perform parameter estimation in SMB systems, as evidenced by these and more examples in literature (Kawajiri and Biegler, 2008; Suzuki, 2022; Chen et al., 2010). Even though both the use of PSO to estimate parameters and parameter estimation for SMB systems are separately well explored, their simultaneous application, that is, adopting (meta-)heuristic methods to explore parameter estimation in a SMB system, is uncommon. As a rather rare example, He *et al.* applied a stochastic MCMC method to solve the proposed optimization study (He et al., 2020). Furthermore, among the few studies employing heuristic methods, only one study, which was conducted by some of the authors of the present work, uses PSO to perform parameter estimation (Santos, 2021). However, this study differs from current one in its methodology, as it employs an estimability analysis and a more comprehensive uncertainty analysis.

The present study aims to leverage experimental data to validate the proposed methodology. This approach enables the estimation of mathematical model parameters through PSO, effectively describing protein separation in a specific case study. In this scenario, an SMB unit packed with Sephadex G-50 as stationary phase was employed to purify essential components. To support this objective, estimation based on fixed bed experiments was conducted to enhance and validate following parameter estimations. Additionally, an estimability analysis was introduced to assess the influence of various parameters on the system. The outcomes of this analysis can be juxtaposed with the phenomenological understanding of the system, offering insights into its consistency. Moreover, the study incorporated data reconciliation to address experimental inconsistencies and conducted uncertainty analysis to develop a more robust model.

As previously noted, parameter estimation for SMB units using meta-

heuristic methods remains underexplored in the open literature. Consequently, comprehensive studies that integrate detailed characterization analyses are even scarcer. This work contributes to the field by introducing a novel optimization methodology for SMB systems, which combines PSO with thorough local estimability and uncertainty analyses to enhance the interpretation and reliability of the yielded results. The selected case study, previously investigated in the literature, provides a point of comparison that supports the validity of the proposed methodology (Rios et al., 2020).

2. Materials and methods

The proteins studied were Myoglobin (Mb) and Bovine Serum Albumin (BSA). Myoglobin, part of the globin family, is mainly responsible for the binding and transport of oxygen in most vertebrates due to the presence of a heme group. Mb has a mass of approximately 17800 Da (Hendgen-Cotta et al., 2014; Essa et al., 2007). BSA, derived from bovine sources, is the most abundant protein in blood plasma. It is smaller than other blood proteins, and is notable for its high solubility and stability (Peters, 1970). The BSA molecule consists of 563 amino acids, which translates to a substantial mass of 66400 Da, significantly larger than Mb. This difference permits the use of sieve (size exclusion) chromatography for their separation (Peters, 1995). The chromatography stationary phase used, Sephadex G-50, is an organic size exclusion gel with a sieve range spanning from 1500 to 30000 Da, allowing Mb to enter the gel pores, whereas BSA can freely cross the packed bed due to its larger size (Rios et al., 2020).

The mathematical model used in this study was already experimentally validated by the research group previous works for different operating conditions and adsorbents (Rios et al., 2020; Rios et al., 2023; Rios et al., 2023). The model was developed in gPROMS. To prepare it for parameter estimation, the desired parameters to be studied must be set as variables beforehand within the software. Furthermore, the connection between gPROMS and MATLAB® must be built. This link was obtained through the gO:MATLAB function, which facilitates data exchange between the two software tools and provides the necessary means to perform gPROMS simulations using values supplied by MATLAB®.

The structure of the methodology considered for parameter estimation and its validation is presented in Fig. 1. The main goal of this method is to perform simultaneous parameter estimation using both SMB data and fixed bed data. This sequence of tasks was selected because certain parameters are common for both fixed bed and SMB and can be more accurately estimated from fixed bed experiments, yielding more precise values compared to those obtained from SMB experiments. The initial fixed bed estimation provides valuable insights, such as method feasibility and close-to-optimal parameter values, that contribute to the setup and validation of subsequent, more complex estimations, hence the need to perform a fixed bed estimation before a simultaneous SMB + fixed bed estimation. It is crucial, however, that no parameter data or information be directly transferred between estimations, to maintain the integrity and reliability of each individual estimation. As mentioned before, studies where similar methodologies were used were conducted prior to this study, however the algorithms and methodologies employed in those works were more restrictive, as problem-dependent deterministic methods were instead used to solve the proposed optimization problem (Grosfils et al., 2007; Bentley et al., 2013).

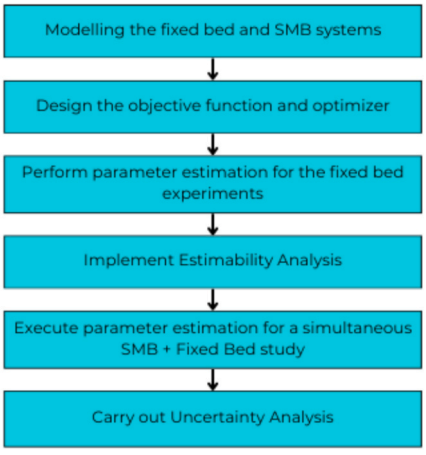

Fig. 1. Structure methodology.

The parameters that simultaneously describe the SMB and fixed bed systems are designated as "common parameters" for the sake of convenience. Hence, this term is used in the remainder of this article.

Size exclusion separation, which occurs within the Sephadex G-50 matrix, is a straightforward process, where the retention time of a component in the column is determined solely by its pore accessibility and no effective adsorption occurs. Additionally, no competition or site inhibition occurs during this separation. Hence, the underlying mechanism is described by a simpler model, requiring fewer parameters to be completely defined. It was considered that the isotherm assumed by Rios and coworkers for the Sephadex G-50 separation, a linear isotherm, was the most suitable for the obtained separation data.

The separation experimental setup and data are detailed in the source work, which is some of the authors' previous work. The datasets used include a Blue Dextran (BD) breakthrough experiment, a Mb breakthrough experiment, a BSA breakthrough experiment, two different binary breakthrough experiments with different feed concentrations, and finally, an SMB experiment, performed for 10 cycles, for a total of six different datasets. All experimental data available from Rios *et al.* was used in this study and can be seen in the figures of the present study (Rios et al., 2020). Due to the nature of the estimation, which has the objective of estimating parameters for a specific set of experimental conditions, it is appropriate to use all available experimental data to ensure that the estimated parameters closely reflect the experimental observations and are as accurate as possible. However, by using all data we may introduce overfitting into our methodology, so it is imperative to also perform an adequate test to ascertain whether this risk is real.

The software used in this study consisted of MATLAB® R2023a Update 1 (9.14.0.2239454) and gPROMS 7.0.7.55178. These were required to build the necessary scripts, formulate the objective functions, and execute the optimization algorithm. The optimization simulations were performed using a desktop computer featuring an Intel® Core™ i9-9900K CPU @ 3.60GHz processor and 32 GB of RAM.

2.1. Fixed bed modelling

For the fixed bed experiments, the model employed was considered isothermal, assuming a constant mobile phase velocity (diluted mixtures) and the absence of interactions between solutes. The gel's particles were considered spherical and uniform. Additionally, plug-flow with axial dispersion was considered for the movement of the fluid phase (Rios et al., 2020). With these assumptions, the mass balance to the fluid phase, considered for this model, is as follows:

$$\frac{\partial C_i}{\partial t} = D_{ax}\frac{\partial^2 C_i}{\partial z^2} - u_i\frac{\partial C_i}{\partial z} - \frac{(1-\varepsilon_b)}{\varepsilon_b}\frac{\partial \overline{q}_i}{\partial t} \tag{1}$$

where the parameter D_{ax} refers to the axial dispersion coefficient, u_i is the interstitial velocity, ε_b is the fixed bed porosity, C_i is the concentration of protein i in the fluid phase and $\overline{q}_i$ is the average adsorbed concentration of protein i. Lastly, z represents the axial direction. The mass balance to the particles is described by the linear driving force (LDF) equation:

$$\frac{\partial \overline{q}_i}{\partial t} = k_{h,i}\left(q_i^* - \overline{q}_i\right) \tag{2}$$

in which q_i^* is the adsorbed concentration in equilibrium with the fluid phase concentration of protein i, while $k_{h,i}$ is the mass transfer coefficient.

Lastly, the equilibrium relation between the liquid and solid phases can be represented by the following expression, equivalent to a linear isotherm equation:

$$q_i^* = K_{SEC,i} C_i \tag{3}$$

where $K_{SEC,i}$ is the size exclusion constant.

To correctly simulate the model, the following initial and boundary conditions were considered:

Initial Conditions:

$$t = 0 \rightarrow C_i = \overline{q}_i = 0 \tag{4}$$

Boundary Conditions:

$$z = 0 \rightarrow D_{ax}\frac{\partial C_i}{\partial z} = u_i\left(C_i - C_i^F\right) \tag{5}$$

$$z = L \rightarrow \frac{\partial C_i}{\partial z} = 0 \tag{6}$$

with L being the column length and C_i^F being the concentration of protein i at the feed inlet.

The parameter Q_{feed} pertains to the feed flow rate for the fixed bed column, and can be obtained through the following expression:

$$u_i = \frac{Q_{feed}}{A\varepsilon_b} \tag{7}$$

where A is the known area of the column cross-section.

The set of estimable parameters for the fixed bed experiments were $\theta_1 = [\varepsilon_b, D_{ax}, Q_{feed}, K_{SEC,i}, k_{h,i}]$, with i pertaining to the studied protein, totaling 5 parameters when studying individual protein cases, and 7 parameters for the binary mixture cases.

2.2. SMB modelling

For the SMB experiments, it is possible to utilize the already available fixed bed model as the individual columns and incorporate the necessary mass balance to the nodes. Furthermore, the model should include the necessary global balances and represent the structure of the additional equipment involved, such as pipes and manifolds.

The global balances are described by the following expressions:

$$Q_I = Q_D + Q_{IV} \tag{8a}$$

$$Q_{II} = Q_I - Q_X \tag{8b}$$

$$Q_{III} = Q_{II} + Q_F \tag{8c}$$

$$Q_{IV} = Q_{III} - Q_R \tag{8d}$$

where *I, II, III,* and *IV* represent the section of the SMB equipment, and the subscripts *D, F, R,* and *X* are related to the desorbent, feed, raffinate, and extract streams, respectively. From (8a) to (8a), it is possible to obtain the ensuing equation:

$$Q_D + Q_F = Q_X + Q_R \tag{9}$$

The expressions that follow accurately depict the mass balances of the SMB equipment at the inlet/outlet nodes or between columns:

$$\textbf{Desorbent node}: C_{i,I}^{in} = \frac{Q_{IV}C_{i,IV}^{out}}{Q_I} \tag{10a}$$

$$\textbf{Extract node}: C_{i,II}^{in} = C_{i,I}^{out} \tag{10b}$$

$$\textbf{Feed node}: C_{i,III}^{in} = \frac{\left(Q_{II}C_{i,II}^{out} + Q_F C_{i,F}\right)}{Q_{III}} \tag{10c}$$

$$\textbf{Raffinate node}: C_{i,IV}^{in} = C_{i,III}^{out} \tag{10d}$$

$$\textbf{Between columns}: C_{i,k}^{in} = C_{i,k-1}^{out} \tag{10e}$$

To account for the transport of material between columns or before/after the inlet/outlet ports, where no separation occurs, transfer lines were introduced into the SMB model, in which plug-flow is assumed; therefore, dead volumes of the system were also considered.

For the SMB modelling, the axial dispersion coefficient for each column is instead estimated through the Peclet number, yielded by the following expression:

$$Pe_j = \frac{u_i L}{D_{ax_j}^{SMB}} \tag{11}$$

Therefore, the set of chosen parameters for the common parameter estimation were $\theta_2 = [\varepsilon_b, D_{ax}, Q_{feed}, K_{SEC,i}, k_{h,i}, \varepsilon_{b_j}^{SMB}, Pe_j, Q_F, Q_D, Q_E, Q_{IV}]$ with i referring to the studied protein and j is the column number (1,2, …,6), totaling 23 estimable parameters. Even though flow parameters (Q_F, Q_D, Q_E, Q_{IV}) are susceptible to changes, due to pump pulsations or port switch interruptions for example, these changes were considered negligible when compared to the average value, and so, the assumption that these parameters are constant throughout the experiments was considered an accurate approximation. Estimating these variations would introduce an increase in computational effort due to an increase in parameters to estimate and could make the problem much more prone to estimability issues, resulting from possible correlations and/or low parameter influence. Dead volumes could also be considered for estimation, since the dead volumes present in the unit can be detrimental to the SMB simulation results. However, in this work, these elements were not considered for estimation since the size of these elements was considered known from previous studies (Rios et al., 2020) and its variation negligible. Therefore, the inclusion of the dead volumes in the chosen parameter set would also increase the computational cost unnecessarily and so their study was considered nonessential.

2.3. Particle swarm optimization

While the core concept of PSO remains the same, different algorithms may be employed depending on the type of problem to which this technique is applied. Due to the relatively simple nature of the optimization problem at hand, and to avoid increasing unnecessarily the computational effort, a simple PSO algorithm was employed and will be detailed in this sub-section.

The optimization algorithm starts with an initialization step, where a position x is randomly given to each particle:

$$x_{1,k,n} = x_{min}(n) + r^*\left(x_{max}(n) - x_{min}(n)\right) \tag{12}$$

in which k shows the particle number, and n denotes the decision variable. The variable r^* is a random number between 0 and 1. The variables x_{max} and x_{min} pertain to the upper and lower position bounds for each decision variable n. The maximum velocity achievable by the particles in this process is also defined in this step and is equivalent to the upper limit of the particles position for the variable in question ($v_{max} = x_{max}$).

Once the positions of each particle have been determined, the next step involves calculating the objective function. Subsequently, the best positions yielded by each individual particle, P_{best}, and the overall best position obtained by the swarm, G_{best}, up to the current iteration, are updated and archived. The decision of the best positions is based on the

lowest objective function value yielded by the particles.

The next step encompasses a value update for the acceleration coefficients. These parameters will evolve as follows:

$$\omega_{O,j}^{*} = \omega_{O,j} + \frac{(C_{f,j} - \omega_{O,j})^{*} i}{N_{iter}} \tag{13}$$

where i represents the iteration and $j = 1,2$, is an index indicating the coefficients' nature to ascertain if the search is global (1) or local (2). $\omega_{O,j}^{*}$ is the updated value of the acceleration coefficient to be used in the current iteration, while $\omega_{O,j}$ is the value utilized in the previous iteration. In the first iteration, *i.e.*, $i = 1$, $\omega_{O,j}^{*} = \omega_{O,j}$. The learning coefficients, $C_{f,j}$, are given distinct values, depending on the necessity to pursue global search (higher value for $C_{f,1}$) or local search (higher value for $C_{f,2}$). A balanced search will have learning coefficients with similar values. Finally, N_{iter} corresponds to the total number of iterations employed in the PSO algorithm. In this case, the values $C_{f,1} = 2.5$, $C_{f,2} = 0.5$, $\omega_{O,1} = 0.5$, and $\omega_{O,2} = 2.5$.

Following this step, velocities are then calculated:

$$v_{i,k,n} = \omega_{O,1}^{*} r_1 \left(x_i^{G_{best}} - x_{i-1,k,n} \right) + \omega_{O,2}^{*} r_2 (x_i^{P_{best}} - x_{i-1,k,n}) \tag{14}$$

where r_1 and r_2 are random numbers between 0 and 1. It is important to note that the constraint $v_{i,k,n} \leq v_{max}$ must be satisfied. If the constraint is violated, the new velocity will be set to the maximum velocity value, ensuring that the constraint is once again complied with. If the computed velocity is equal to zero, a pseudo-random velocity is given to the particle. This given velocity considers the iterations already completed, so that, as the optimization proceeds, the possible maximum pseudo-random velocity diminishes.

The particle position is then updated using the following equation:

$$x_{i,k,n}^{*} = v_{i,k,n} + x_{i-1,k,n} \tag{15}$$

The new position must not compromise the feasible region's limits, therefore $x_{min} \leq x_{i,k,n}^{*} \leq x_{max}$. Once again, when this constraint is violated, the new positions will assume boundary values, *i.e.*, $x_{i,k,n}^{*} = x_{min}$ or $x_{i,k,n}^{*} = x_{max}$ depending on the type of boundary. If the constraints are satisfied, then $x_{i,k,n}^{*}$ is the particle position for the next iteration.

Lastly, if k is less than the total number of particles (N_p), the algorithm repeats until all particles have been analyzed. Once this is concluded, if i is less than the total number of iterations (N_{iter}), all the steps are repeated until the designated number of iterations has been reached. Afterward, key outputs such as the minimum objective function value and the corresponding decision variable values can be identified.

To apply a PSO algorithm effectively, it is imperative to select an appropriate number of particles (N_p) and iterations (N_{iter}) to ensure convergence without excessive computation time. Furthermore, suitable values for other PSO parameters, such as the acceleration and learning coefficients, must also be chosen on whether a global, local, or a balanced search is desired. Additionally, the number of decision variables (N_{DV}) and their respective lower and upper position bounds must also be properly established to construct a feasible optimization region.

2.4. Objective function

The objective functions minimized by the PSO algorithm were designed to find parameter values that would reduce the residuals between the generated mathematical model and the experimental data.

The decision variables for this optimization problem are the parameters in the θ sets, described in Sections 2.1 and 2.2. The only constraints are the defined bounds for each one of the parameters belonging to these sets.

Each experiment used for parameter estimation was simulated using the "gO:MATLAB" command, enabling MATLAB® to call the gPROMS software to perform the desired simulations. The parameter values used in the simulations were determined by the positions of each decision variable $(x_{i,k,n})$ from the PSO algorithm. The experimental data collected in a previous study (Rios et al., 2020) was imported to MATLAB® and organized in a predefined matrix.

The objective function that describes the optimization problem is based on a Mean Squared Error (MSE) function, and is described as follows:

$$\min_{\theta} \frac{1}{N} \sum_{j=1}^{N_s} \omega_j \sum_{i=1}^{N_j} \left(y_{exp,i,j} - y_{sim,i,j}(\theta) \right)^2 \tag{16}$$

Subject to:

$$x_{min} \leq \theta \leq x_{max} \tag{17}$$

where N_j is the number of times this mismatch is calculated for a particular experiment j, which coincides with the number of experimental data points for said experiment, $y_{sim,i,j}$ represents the simulated data, $y_{exp,i,j}$ pertains to the experimental data, N_s refers to the number of experiments considered in the estimation procedure, ω is a weighing factor for the considered experiment, computed so that every experiment has the same weight within the minimization context, regardless of number of experimental points, and N is the total number of differences calculated throughout all experiments and can be obtained through the following equation:

$$N = \sum_{j=1}^{N_s} N_j \tag{18}$$

Equation (16) implies that a lower objective function value indicates a better alignment between the experimental data and the model. Since the error function is based on the MSE, deviations at higher concentration values have a greater impact, while those at low concentrations contribute less. A constant level of measurement noise was assumed across all data points and, as a result, smaller deviations likely related to this noise, given their magnitude is comparable to the standard deviation of the measurement error. In contrast, larger deviations suggest a model-data mismatch.

Nevertheless, the MSE was considered an appropriate and sufficient choice for the goal at hand.

However, to offer a quick point of reference using a more commonly encountered performance metric, the coefficient of determination, R^2, shown in equation (19), is also provided.

$$R^2 = 1 - \frac{SS_{Res}}{SS_{tot}} \tag{19}$$

In this equation, SS_{Res} is the sum of squares of residuals, and is given by $\sum_i \left(y_{exp,i} - y_{sim,i} \right)^2$ and SS_{tot} is defined by $\sum_i \left(y_{exp,i} - \overline{y_{exp}} \right)^2$. While the MSE function remains the main metric guiding parameter estimation in this study, R^2 serves as a complementary indicator that helps contextualize the quality of the model fit in a way that is more broadly used. The values will be displayed in the captions of the appropriate figures.

2.5. Estimability analysis

The estimability analysis employed in this work is a local sensitivity technique based on the Gram-Schmidt principle of orthogonalization. This analysis was conducted to identify potential correlations between parameters, as well as parameters with negligible influence on the model output that could compromise accurate estimation. A favorable estimability analysis can lead to a more streamlined estimation process by eliminating unnecessary parameters. For this task, the technique employed is shown to be effective.

Each parameter, S_i, has an assigned sensitivity vector, S_i'. The selection process involves identifying the parameter with the highest

sensitivity, after which the remaining vectors are represented orthogonally in the plane perpendicular to the chosen parameter's sensitivity vector. This will be iterated until all parameters are selected or until the sensitivity of the largest parameter falls below a predefined cut-off value (Kravaris et al., 2013).

Using this methodology, the initial step is to create the sensitivity matrix.

Considering the following expression:

$$y = f(x(t), \theta, t) \tag{20}$$

in which y is the vector that holds the outputs, $x(t)$ is the vector of state variables, θ is the vector of model parameters, and t is the time, the sensitivity matrix coefficients can be determined using the following expression:

$$S'_{i,p}\Big|_{t=t_n} = \frac{\theta_p}{y_i}\frac{y_i(t,\theta_p+\Delta\theta_p)-y_i(t,\theta_p)}{\Delta\theta_p}\Bigg|_{t=t_n} \tag{21}$$

with $i = 1,2,\ldots,N_y; p = 1,2,\ldots,N_p; n = 1,2,\ldots,N_t$ and where y_i is the i-th output obtained through the model, θ_p, is the parameter p, and t_n is the time instant evaluated. The constant N_y is the number of output variables, N_p is the number of parameters, and N_t is the number of chosen time-steps. Notably, the coefficients are normalized to account for the differing orders of magnitude among parameters. This ensures that all parameters contribute equally to the analysis, as those with smaller magnitudes may exhibit larger values of the derivatives of the model outputs with respect to those parameters, while those with larger magnitudes are expected to have smaller values of the derivatives with respect to those parameters. These calculations result in a sensitivity matrix S:

$$S = \begin{vmatrix} S'_{1,1}\big|_{t_1} & \cdots & S'_{1,N_p}\big|_{t_1} \\ \vdots & \ddots & \vdots \\ S'_{1,1}\big|_{t_n} & \cdots & S'_{1,N_p}\big|_{t_n} \\ \vdots & & \vdots \\ S'_{N_y,1}\big|_{t_1} & \cdots & S'_{N_y,N_p}\big|_{t_1} \\ \vdots & \ddots & \vdots \\ S'_{N_y,1}\big|_{t_n} & \cdots & S'_{N_y,N_p}\big|_{t_n} \end{vmatrix}_{N_y N_t \times N_p} \tag{22}$$

A computation of the magnitude of each column is then performed:

$$M(p) = S_p^T S_p \tag{23}$$

In the expression above, S_p is the column p of the sensitivity matrix, while T denotes the transpose of the associated vector. Through equation (23), it is possible to determine the parameter that has the highest magnitude and consequently, the highest influence in the final model, S_{max}. It is then necessary to project matrix S in relation to this column, resulting in matrix S_0:

$$S_0 = S_{max}(S_{max}^T S_{max})^{-1} S_{max}^T S \tag{24}$$

The residual matrix, R, is then computed using both matrices S and S_0:

$$R = S - S_0 \tag{25}$$

Upon obtaining R, the magnitude of its columns is calculated, and the next parameter is chosen as the reference for orthogonalization. This iterative process continues until all parameters are analyzed or the highest magnitude falls below a predefined tolerance value, which can be chosen arbitrarily.

This analysis helps remove correlated or low-impact parameters, leading to a simplification of the optimization problem. However, a subsequent analysis using Hessian matrices is required to ensure mathematical certainty regarding the selected estimable parameters' ability to yield an optimum.

A reasonable approximation of the Hessian matrix, H, can be derived through the coefficients of matrix S_f. This matrix is similar to the sensitivity matrix S; however, it exclusively includes the parameters identified as estimable through the orthogonalization methodology. Thus, the approximation of the Hessian matrix is obtained through the following expression:

$$H = 2S_f^T S_f \tag{26}$$

An eigenvalue calculation proceeds. A positive-definite Hessian matrix confirms that the region defined by the selected parameters will yield a strict local minimum. If the matrix is not positive-definite, there is a lack of mathematical proof of convergence or even the existence of an optimum within the region (Nogueira and Pontes, 2017). However, the Hessian approximation presented above invariably yields a positive-definite or semi-definite matrix, the latter allowing for the possibility of directions of nonincreasing objective function at the minimum. Nonetheless, this level of approximation was considered sufficient for the present purpose, as the primary objective is to assess the existence of a strict local minimum within the explored region.

2.6. Uncertainty evaluation

For the uncertainty analysis, various methodologies could be employed to comprehensively characterize the results. Given the available resources, an approach based on the Hessian matrix could be considered. However, since PSO provides several optimization instances that are pseudo-dependent, the following methodology was assumed to be more precise among the available alternatives, as it leverages the full set of information generated by the optimization algorithm.

Throughout the PSO, all particle positions, $x_{i,k,n}$, were archived. However, only those that fulfil the Fisher-Snedecor test, the expressions of which are shown below, may be utilized in the uncertainty evaluation. The equations pertaining to the test were already deduced in literature (Santos, 2021; Rebello et al., 2021; Benyahia et al., 2013).

$$F_{obj}(\theta) < F_{test} \tag{27}$$

$$F_{test} = F_{obj}^{opt} \bullet [1 + C_{conf}] \tag{28}$$

$$C_{conf} = \sqrt{\frac{N_m(N_p+N_y-1)}{N_m-N_p-N_y-1} \bullet F_{\alpha_{cov}}(N_p+N_y-1, N_m-N_p-N_y-1)} \tag{29}$$

These equations utilize known coefficients, such as the number of parameters, the number of output variables and the number of measurements, N_p, N_y and N_m, respectively, to obtain a confidence coefficient, C_{conf}, that enables the determination of particles that pass the Fisher-Snedecor test (F_{test}). The parameter $F_{\alpha_{cov}}$ is the Fisher function that depends on the degrees of freedom of the problem at hand, while F_{obj}^{opt} is the objective function value at the optimum of the global particle swarm.

To quantify the uncertainty of each parameter p, u_p, the following expression was utilized:

$$u_p = K \times \sqrt{\frac{1}{N-1}\sum_{i=1}^{N}\left(\theta_{i,p}^{PSO} - \overline{\theta}_p\right)^2} \tag{30}$$

$$\overline{\theta}_p = \frac{1}{N}\sum\nolimits_{i=1}^{N} \theta_{i,p}^{PSO} \tag{31}$$

in which i refers to a particle number, where the total number of particles is the number of particles per iteration times the number of iterations, K is the coverage factor, which was assumed to be 2

(approximately 95% of confidence, since the PSO particles were assumed to follow a Gaussian distribution), $\bar{\theta}_p$ is the average value yielded by all PSO particles for each parameter according to equation (31), $\theta_{i,p}^{PSO}$ are all the values yielded by the PSO for each parameter, and N is the total number of values obtained for each parameter, which coincides with the number of PSO particles that fulfilled the Fisher-Snedecor test. Moreover, $\theta_{i,p}^{PSO}$ also only considers values that fulfilled the Fisher-Snedecor test.

The propagation of the uncertainty, U_c, into the final model can also be determined as follows:

$$U_c = \sqrt{\frac{\sum_{p=1}^{N_p} u_p{}^2}{\left(\sum_{p=1}^{N_p} X_p\right)^2}} \tag{32}$$

in which X_p is a vector with the best values for each parameter yielded by the PSO.

Monte Carlo simulations may be performed to better characterize the results obtained. These simulations can be executed by sampling parameter values from a normal distribution, shown in equation (33), with $\mu = \bar{\theta}_p$ and standard deviation $\sigma_p = \frac{u_p}{K}$.

$$f(x) = \frac{1}{\sqrt{2\pi\sigma_p^2}} exp^{-\frac{(x-\mu)^2}{2\sigma_p^2}} \tag{33}$$

3. Results

3.1. Fixed bed parameters estimation

To effectively study and determine the parameters for the separation process under consideration, first, an analysis was performed on independent fixed bed experiments. This analysis entailed the implementation of a PSO with $N_p = 100$ and $N_{iter} = 100$. The selection of the number of iterations and particles, for this experiment and the subsequent ones, was guided by a balance between achieving optimal convergence and minimizing computational time and supported by preliminary time extrapolation studies conducted prior to the estimation runs. The chosen values enabled the acquisition of a set of parameters that would create a mathematical model with a minimal residual alignment with the experimental data from the fixed bed experiments within a reasonable time. The estimated parameters yielded in this step would then serve as reference parameters for further estimations.

The estimated parameters sets are compiled in Tables 1–3, alongside the parameters of the mathematical model obtained experimentally by Rios and coworkers (Rios et al., 2020). The methodology employed here, in contrast to Rios *et al.* work, obtains the parameters' values through computational, optimization-based parameter estimation. Additionally, the value of the objective function of each set can be observed in these tables.

It is possible to observe that the estimated axial dispersion coefficient, D_{ax}, constantly has a value below the one determined through previous experimental work. This implies that this parameter is slightly lower than what was previously assumed. Bed porosity, ε_b, also reveals a slight increase in every experiment. Other parameters, such as the feed flow, Q_{feed}, and the size exclusion constants, $K_{SEC,BSA}$ and $K_{SEC,Mb}$, show slight deviations to the values obtained by Rios *et al.*, but still within the range that was expected. The mass transfer coefficients yield values with no recognizable patterns in their deviations throughout the test and final estimations performed. This phenomenon suggests that these parameters have very low effect in the output model, and there is a considerable range of values for these coefficients that can yield close-to-optimal objective function values. This was somewhat expected, and the reason will be provided in the following sub-section, after definitive proof for this postulation is given.

Since the objective function values obtained for all cases are lower for the sets of estimated parameters, it is concluded that these sets generate models with better alignment to the experimental data than the set with parameters yielded by previous experimental work. Figs. 2–5 present a graphical comparison between the experimental data points and the mathematical model generated with Rios' parameters and with the estimated parameters. While only slight variations can be observed, these differences corroborate the prior conclusion.

Table 1
Rios' and estimated set of parameters for the Mb experiment.

Parameter	Rios' Parameters' values	Estimated Parameters'values
ε_b	0.390	0.395
$D_{ax}(m^2 \bullet s^{-1})$	3.83 x 10^{-7}	3.28 x 10^{-7}
$Q_{feed}(m^3 \bullet s^{-1})$	3.17 x 10^{-8}	3.25 x 10^{-8}
K_{SEC}	0.300	0.333
$k_h(s^{-1})$	0.175	0.999
f_{obj}	1.23 x 10^{-5}	5.01 x 10^{-6}

Table 2
Rios' and estimated set of parameters for the BSA experiment.

Parameter	Rios' Parameters' values	Estimated Parameters'values
ε_b	0.390	0.391
$D_{ax}(m^2 \bullet s^{-1})$	3.83 x 10^{-7}	5.40 x 10^{-8}
$Q_{feed}(m^3 \bullet s^{-1})$	3.17 x 10^{-8}	3.16 x 10^{-8}
K_{SEC}	0	0.028
$k_h(s^{-1})$	0.0564	0.03018
f_{obj}	1.46 x 10^{-1}	3.26 x 10^{-2}

Table 3
Rios' and estimated set of parameters for the binary experiments.

Parameter	Rios' Parameters' values	Estimated Parameters' values
ε_b	0.390	0.395
$D_{ax}(m^2 \bullet s^{-1})$	3.83 x 10^{-7}	9.74 x 10^{-8}
$Q_{feed}(m^3 \bullet s^{-1})$	3.17 x 10^{-8}	3.17 x 10^{-8}
$K_{SEC,BSA}$	0	0.015
$K_{SEC,Mb}$	0.3	0.298
$k_{h,BSA}(s^{-1})$	0.056	0.566
$k_{h,Mb}(s^{-1})$	0.175	0.047
f_{obj}	0.0151	0.0107

3.2. Estimability analysis

An estimability analysis was conducted for each of the fixed bed experiments. This analysis aimed to quantify and compare the impact of the parameters in the final model amongst others within the parameter set. Moreover, it sought to detect significant correlations among parameters that would hinder the parameter estimation process, and in the process, eliminate parameters from the optimization problem that would impede the estimation, simplifying it before tackling a more complex problem that also includes SMB experiments. This information can all be obtained through the generated magnitudes. These are presented below in Table 4and Table 5 for the single experiments and Table 6 for the binary experiment. Highlighted cells correspond to the columns (parameters) with the highest magnitudes for each iteration, serving as references for the orthogonalization in that particular iteration.

Across all experiments, it is possible to observe minor correlations between parameters, since there is a slight variation in the magnitude of the columns associated with the correlated parameters whenever the sensitivity matrix, S, is orthogonalized. Nevertheless, this variation was deemed insignificant, so no correlation that would inhibit a successful and correct estimation was identified. Moreover, the column flow rate, whether in fixed bed or SMB columns, was assumed constant throughout

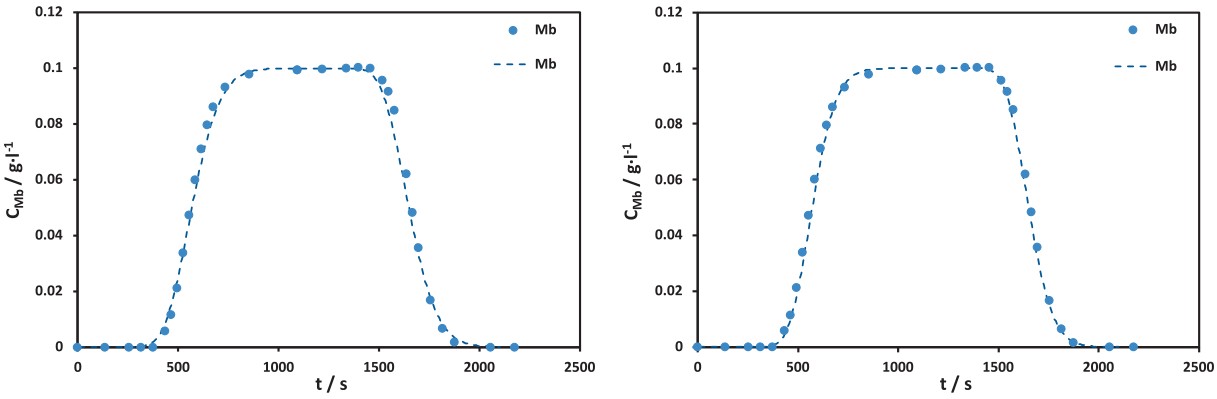

Fig. 2. Graphical comparison between Mb experimental data (points) and the models (dashed lines) generated with Rios' parameters (left) (R^2 – 0.9956) and the estimated parameters (right) (R^2 – 0.9980).

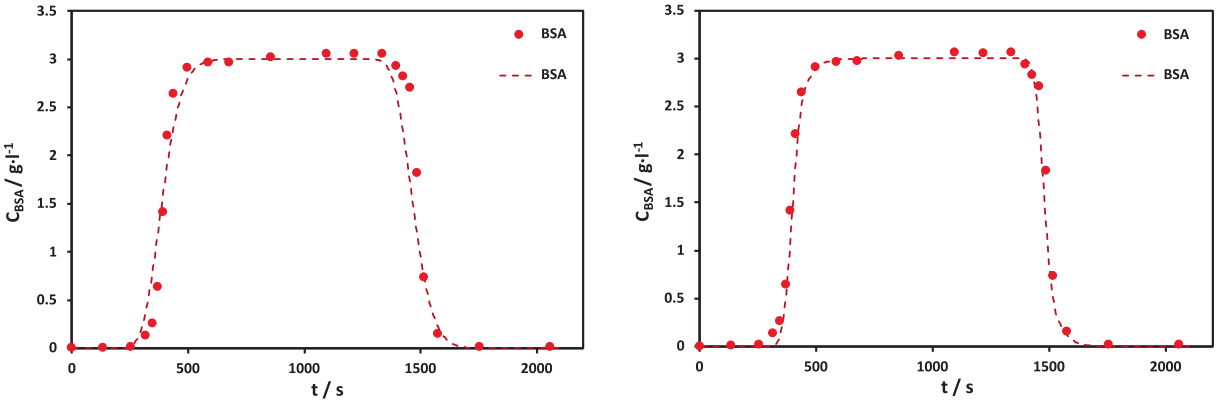

Fig. 3. Graphical comparison between BSA experimental data (points) and the models (dashed lines) generated with Rios' parameters (left) (R^2 – 0.9402) and the estimated parameters (right) (R^2 – 0.9879).

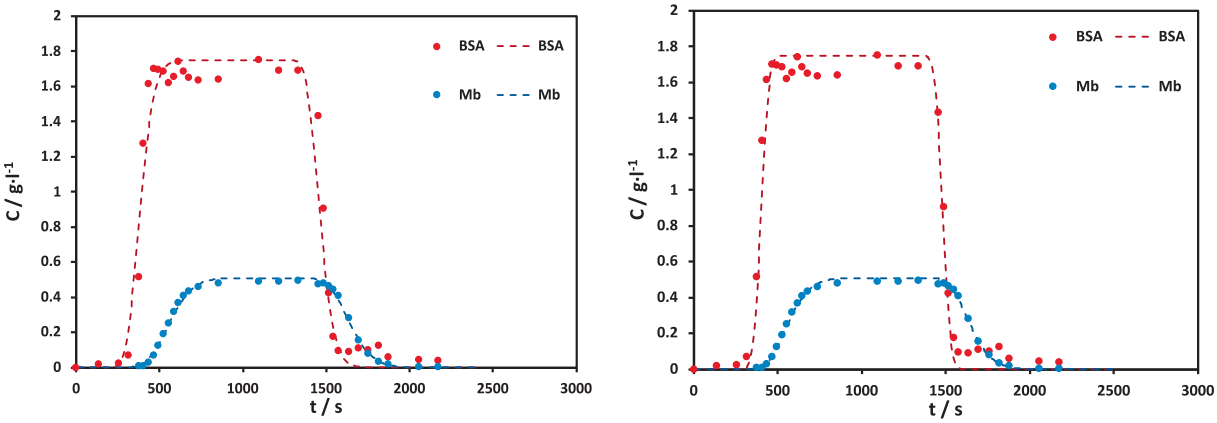

Fig. 4. Graphical comparison between the binary experimental data (points) and the models (dashed lines) generated with Rios' parameters (left) (R^2 Mb – 0.9956; R^2 BSA – 0.9676) and the estimated parameters (R^2 Mb – 0.9971; R^2 BSA – 0.9888) (right)– Exp. 1.

the column length. Additionally, the PSO search range for this parameter was narrowly constrained ($\pm$ 0.05 $\times$ 10^{-8} $m^3 \bullet s^{-1}$), limiting its variability. While minor correlations with other parameters may exist, any influence is expected to be negligible.

Any magnitude below the predefined cut-off value, 100, was not considered as reference for orthogonalization and, when reached, implied the end of the estimability analysis.

As expected, the magnitude of the column corresponding to the mass transfer coefficients, $k_{h,i}$, consistently fell below the established cut-off value in each iteration, for all experiments. This finding indicates that the effect of this parameter in the resulting model is nearly negligible, corroborating the postulation in the previous section. In local estimability analysis, a low magnitude may also imply that the parameter value is close to an optimum, so small changes have little to no effect on the model. However, in this case, the relatively low magnitude may be caused by the nature of the experiments itself. These experiments are governed by equilibrium instead of kinetics. Therefore, the kinetic parameters $k_{h,i}$, when compared with equilibrium parameters, such as

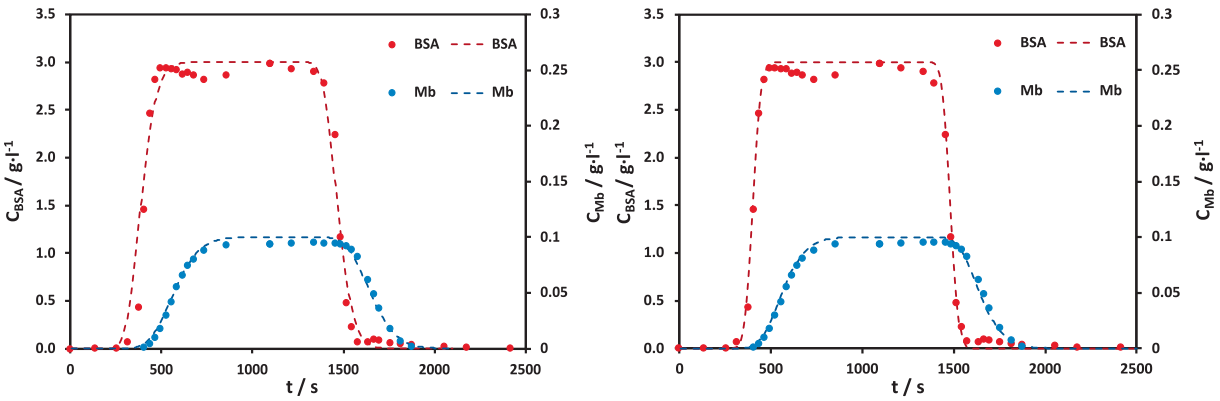

Fig. 5. Graphical comparison between the binary experimental data (points) and the models (dashed lines) generated with Rios' parameters (left) (R^2 Mb – 0.9922; R^2 BSA – 0.9739) and the estimated parameters (right) (R^2 Mb – 0.9893; R^2 BSA – 0.9968) – Exp. 2.

Table 4
Magnitudes at each iteration for the Mb fixed bed experiment.

Iteration	ε_b	D_{ax}	Q_{feed}	K_{SEC}	k_h
1	5.35 x 10^7	3.36 x 10^6	1.21 x 10^9	6.63 x 10^3	7.45
2	8.00 x 10^6	3.33 x 10^6	-	6.62 x 10^3	7.48
3	-	3.20 x 10^6	-	5.96 x 10^3	7.06
4	-	-	-	5.96 x 10^3	6.24
5	-	-	-	-	6.04

Table 5
Magnitudes at each iteration for the BSA fixed bed experiment.

Iteration	ε_b	D_{ax}	Q_{feed}	K_{SEC}	k_h
1	8.34 x 10^6	3.82 x 10^6	1.19 x 10^7	2.40 x 10^3	0.416
2	5.68 x 10^4	1.58 x 10^6	-	2.38 x 10^3	0.138
3	5.38 x 10^4	-	-	2.27 x 10^3	0.132
4	-	-	-	7.32 x 10^2	0.018
5	-	-	-	-	0.017

Table 6
Magnitudes at each iteration for the binary fixed bed experiment.

Iteration	ε_b	D_{ax}	Q_{feed}	$K_{SEC,BSA}$	$K_{SEC,Mb}$	$k_{h,BSA}$	$k_{h,Mb}$
1	2.97 x 10^6	9.51 x 10^7	2.66 x 10^6	2.55 x 10^6	4.96 x 10^4	0.919	23.6
2	2.97 x 10^6	-	2.63 x 10^6	2.51 x 10^6	4.94 x 10^4	0.904	23.5
3	-	-	8.42 x 10^5	1.67 x 10^6	4.71 x 10^4	0.671	22.4
4	-	-	6.59 x 10^5	-	4.50 x 10^4	0.436	22.1
5	-	-	-	-	4.21 x 10^4	0.389	22.1
6	-	-	-	-	-	0.389	17.6

$K_{SEC,BSA}$ and $K_{SEC,Mb}$, are expected to have little to no influence. Nonetheless, in experiments where kinetics govern, the influence of mass transfer coefficients will obviously rise.

To ensure that removing these parameters from subsequent estimations would not affect the capacity of the estimations to yield a local minimum for the objective function, an analysis involving the approximation of the Hessian matrix was performed following the methodology described in section 2.5. Table 7 displays the eigenvalues generated from each experiment.

The positiveness of all generated eigenvalues implies that the Hessian matrices are positive-definite and provide mathematical proof that a local minimum exists within the region defined by the estimable parameters. Hence, based on the examination of the results obtained thus far, it was determined that the mass transfer coefficients, $k_{h,i}$, would be assigned fixed values, equal to those obtained by Rios and coworkers (Rios et al., 2020).

3.3. Common parameters estimation

The primary goal of this estimation is, if possible, to identify a set of parameters that could generate a mathematical model that is capable of simultaneously fitting both the SMB experimental data and the fixed bed experimental data. Additionally, a BD fixed bed experiment was also incorporated into this estimation to enhance the estimation of the fixed bed porosity, ε_b, and, consequently, to improve the estimation of the size exclusion constants, K_{SEC}, due to the observed minor correlation between these parameters. BD does not interact with Sephadex G-50 since its size is larger than the sieve dimensions of the solid matrix.

A PSO algorithm using $N_p = 50$ and $N_{iter} = 35$ was employed. Although the number of particles and iterations are lower, due to the sheer number of experiments considered, the computational time was higher when compared with the previous study. Nonetheless, the chosen values were deemed satisfactory to generate a result close to the optimum. Table 8 presents the main parameters obtained from Rios' experiments, the estimated common parameters, and their respective objective function values, while Table 9 provides information about parameters pertaining to the SMB columns, Fig. 6 illustrates a graphical comparison between the SMB experimental data and the corresponding mathematical models for the Extract and Raffinate streams, using each set of parameters.

The simulation outputs correspond to cycle average concentrations, yielding one discrete value per cycle. In this figure and in the following figures with SMB data, dashed lines are used solely to display model trendlines and do not imply continuous concentration trajectories.

As observed in Fig. 6, both simulated datasets exhibit deviations from the experimental data. These discrepancies may be attributed to unrecorded variations in operating conditions during unit operation, as well as to unmodeled disturbances, measurement noise, and other sources of random experimental error. Given the structure of the mathematical model, reproducing exactly the increasing/decreasing trends observed in the experimental data may be infeasible, regardless of the parameter values.

The yielded common parameters reveal very similar values to the parameters obtained by Rios and coworkers for the SMB experiment, except the axial dispersion coefficient, D_{ax}. This parameter shows deviation from the experimentally computed parameter while others remain similar to the previous values, something similar to what was perceived in the fixed bed estimations. These small distinctions between parameter values, coupled with the high difference observed for D_{ax},

Table 7
Eigenvalues of the Hessian matrices (from smallest to largest) obtained for each fixed bed experiment.

Eigenvalues	Mb Experiment	BSA Experiment	Binary Experiment
1	1.19×10^{4}	1.40×10^{3}	6.39×10^{4}
2	6.26×10^{6}	6.49×10^{4}	6.18×10^{6}
3	1.70×10^{7}	2.88×10^{6}	2.33×10^{7}
4	2.52×10^{9}	4.51×10^{7}	5.45×10^{7}
5			1.54×10^{8}

generate a lower objective function value for the estimated common parameter set, and, therefore, this set yields a better alignment to the SMB experimental points, which can be seen in Fig. 6. Although it is possible to observe almost no differences in the extract stream, aside from a negligible increase in BSA contamination, in the raffinate stream, the model has a much better adjustment to the data in the initial cycles, which compensates for the slightly worse alignment in the next cycles. Since the goal of the BD experiment was only to aid the estimation of the of the fixed bed porosity, ε_b, and, consequently, the estimation of the size exclusion constants, K_{SEC}, following analysis and comparisons were not made for this experiment and Fig. 7 serves as a demonstration of the data points used and the yielded alignments for the mathematical model with Rios' parameters and the generated common parameters. While no discernible differences can be observed, the objective function decreased from 0.0036 to 0.0005, showing an improvement in the alignment.

An absolute and relative comparison was then performed between the set of common and reference fixed bed model parameters to observe how the common parameters compare to a close-to-optimal adjustment to the fixed bed experiments. The deviations are compiled in Tables 10–12, while graphical comparisons of the models, for each experiment, are shown in Figs. 8–11.

From the values obtained, it is possible to infer that there are common parameters that reveal deviation from their reference counterpart. In the Mb experiment, the axial dispersion coefficient, D_{ax}, displays a high relative deviation, while other parameters remain similar to the reference ones. This variation leads to a decrease in curvature of the outputs of the resulting model, which consequently translates into a worse alignment to the experimental data, as can be seen in Fig. 8. In the BSA and binary experiment, both the axial dispersion coefficient, D_{ax}, and the size exclusion constant for the BSA protein, $K_{SEC,BSA}$, reveal distinct values than those generated in the fixed bed estimation, particularly in the binary one. Due to the nature of the axial dispersion coefficient and size exclusion constant values, specifically their relatively low absolute value and order of magnitude, even big relative deviations can possibly be caused by small absolute deviations that may have no significant physical consequences in the protein separation. While in the Mb experiment some deviations appear, in both the other experiments no distinctions can be observed, even with relative deviations above 100%.

Finally, the values of the objective functions were then compiled and compared among Rios', reference, and common parameters, to summarize the results obtained throughout the study and understand which set yielded the mathematical model with best alignment to the fixed bed experimental data. Tables 13–15 compile this information.

In the Mb experiment, as expected from the graphical results, the worst alignment was generated by the common parameter set, since the curvature of the model outputs does not match the experimental data accurately, in contrast to the models computed by the other parameter sets. Hence, the common parameter set has the highest objective function value among the three sets and the simultaneous adjustment with the SMB experiment is, in this case, relatively poor. As expected, the reference parameters set has the lowest objective function value, and so, generate the best alignment to the experimental data.

For the BSA and binary experiments, it is possible to observe that Rios' parameters offer the worst alignment to the experimental points, since the set possesses the highest objective function value. The common parameters set's objective function value reveals an intermediate value among the reference and Rios' parameters sets, suggesting a successful simultaneous alignment with the SMB experiment. Once again, as expected, the reference set offers the best adjustment to the data available.

Based on these considerations, it can be concluded that simultaneous parameter estimation for both fixed bed and SMB experiments is feasible, even though the Mb experiments yield a less accurate fit. These discrepancies likely arise because the parameters obtained via the PSO algorithm are inadvertently more optimized for the BSA and binary experiments due to smaller concentration values in the Mb experiments. Therefore, slightly different parameter values, still in the optimal range, could reduce deviations in the Mb experiments, albeit potentially increasing deviations in the others. This could be achieved by changing the values of the objective function weighing factors so that the MB experiments have a slightly higher influence. Nevertheless, this outcome supports the conclusion that the proposed methodology enables satisfactory simultaneous parameter estimation.

To evaluate whether a separation of training and test data was necessary, and to investigate the potential occurrence of overfitting, an 80/20 split of the available data was performed. This was done by assigning the second and seventh of the ten SMB experimental data points (one per cycle), for each species, to the test set, while the remaining points were used for training. This selection was intended to capture as much information as possible about how the separation evolves across cycles within each dataset. Parameter estimation was then carried out on the training set using a PSO algorithm configured with 50 particles and 35 iterations, consistent with the setup employed in the main common parameter estimation procedure.

The estimation results obtained with the reduced training dataset closely matched those of the full-data estimation. In particular, the PSO algorithm converged to a value of the objective function nearly identical to the one yielded by the main common parameter estimation. For the training data, the objective function reached 0.0013 (truncated at four decimal places). When these estimated parameters were subsequently applied to the test set, the objective function was found to be 0.0012, a slightly smaller value than that obtained for the training set. The following figure presents the experimental training and test datasets together with the results of parameter estimation performed on the training set. In addition, a superimposed boxplot on the test datapoints is included in Fig. 12 to illustrate the predictive uncertainty associated with the model's performance on previously unseen data. This uncertainty was obtained using the methodology detailed in Section 2.6, with 250 Monte Carlo simulations performed.

The similarity of the objective functions across the training and test datasets indicates that the model does not suffer from overfitting under the present conditions. If overfitting had occurred, one would expect the objective function to be significantly smaller for the training data compared to the test data. Moreover, the fact that the objective function values obtained from the different datasets are almost identical to those obtained when using the entire dataset further supports the robustness

Table 8
Rios' and common estimated set of main parameters.

Parameter	Rios' Parameters'values	Estimated Parameters'values
ε_b	0.39	0.392
$D_{ax}(m^2 \bullet s^{-1})$	3.83×10^{-7}	4.83×10^{-8}
$Q_{feed}(m^3 \bullet s^{-1})$	3.17×10^{-8}	3.23×10^{-8}
$K_{SEC,BSA}$	0	0.038
$K_{SEC,Mb}$	0.3	0.308
$Q_F(l \bullet min^{-1})$	0.85×10^{-3}	0.86×10^{-3}
$Q_D(l \bullet min^{-1})$	5.000×10^{-3}	5.015×10^{-3}
$Q_E(l \bullet min^{-1})$	3.1×10^{-3}	3.12×10^{-3}
$Q_{IV}(l \bullet min^{-1})$	1.5×10^{-3}	1.501×10^{-3}
f_{obj}	0.0030	0.0013

Table 9
Other parameters yielded in the common estimation compared with Rios' values.

Parameter	Rios' Parameters' values	Estimated Parameters' values	Parameter	Rios' Parameters' values	Estimated Parameters' values
$\varepsilon_{b,1}$	0.390	0.389	Pe_1	67	50.00
$\varepsilon_{b,2}$	0.390	0.389	Pe_2	67	62.38
$\varepsilon_{b,3}$	0.390	0.390	Pe_3	67	50.02
$\varepsilon_{b,4}$	0.390	0.390	Pe_4	67	96.55
$\varepsilon_{b,5}$	0.390	0.389	Pe_5	67	85.36
$\varepsilon_{b,6}$	0.390	0.389	Pe_6	67	50.12

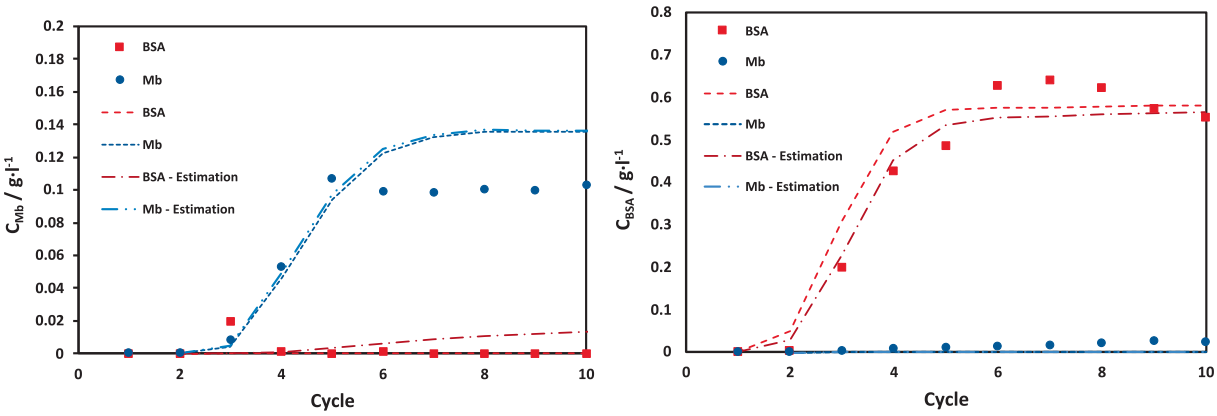

Fig. 6. Graphical comparison between SMB experimental data (points) and the models with Rios' parameters (dashed lines) and estimated parameters (dotted and dashed lines) at the extract (left) and raffinate (right) (R^2 Mb – 0.9140; R^2 BSA – 0.9712).

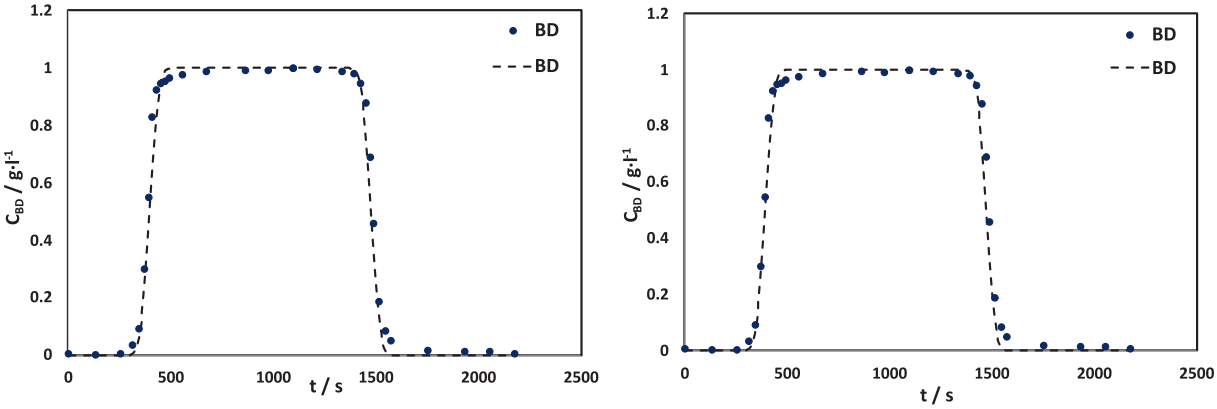

Fig. 7. Graphical comparison between Rios' parameters (left)and estimated parameters yielded by the common parameter estimation (right); experimental data (points); simulated models (dashed lines) – BD experiment.

Table 10
Compilation of deviation between fixed bed parameter and common parameter studies for the Mb experiment.

Parameter	Absolute Deviation	Relative Deviation (%)
ε_b	2.67×10^{-3}	0.68
$D_{ax}(m^2 \bullet s^{-1})$	2.79×10^{-7}	85.2
$Q_{feed}(m^3 \bullet s^{-1})$	1.20×10^{-10}	0.37
K_{SEC}	2.53×10^{-2}	7.59

Table 11
Compilation of deviation between fixed bed parameter and global common parameter studies for the BSA experiment.

Parameter	Absolute Deviation	Relative Deviation (%)
ε_b	9.97×10^{-4}	0.25
$D_{ax}(m^2 \bullet s^{-1})$	5.65×10^{-9}	10.5
$Q_{feed}(m^3 \bullet s^{-1})$	6.93×10^{-10}	2.19
K_{SEC}	9.30×10^{-3}	32.9

of the parameter estimation methodology.

Consequently, these findings suggest that the complete dataset can be employed for parameter estimation without introducing overfitting risks. This is an important outcome, as it ensures that the maximum amount of available information can be leveraged to improve parameter accuracy, ultimately enhancing the methodology's capacity to estimate parameters detailing the underlying system behavior.

3.4. Uncertainty evaluation

The uncertainty computation of the estimable parameters followed the common parameter estimation. By making use of expression (30), it was possible to compute confidence intervals for each parameter. They are compiled in Table 16, alongside the mean values of each parameter throughout the optimization problem, yielded by the PSO:

The best values obtained for the parameters through the PSO procedure and shown in Table 8 fall within their respective confidence

Table 12
Compilation of deviation between fixed bed parameter and global common parameter studies for the binary experiment.

Parameter	Absolute Deviation	Relative Deviation (%)
ε_b	2.63×10^{-3}	0.67
$D_{ax}(m^2 \bullet s^{-1})$	4.91×10^{-8}	50.4
$Q_{feed}(m^3 \bullet s^{-1})$	6.80×10^{-10}	2.15
$K_{SEC,BSA}$	2.21×10^{-2}	143
$K_{SEC,Mb}$	9.81×10^{-3}	3.29

intervals in Table 16. Certain parameters, particularly the Peclet number for each column, may exhibit substantial uncertainty. This is primarily attributable to the very low absolute values of the axial dispersion coefficients in each column, which result in relatively high deviations not having a significant physical impact on protein separation. Consequently, a high degree of uncertainty in these parameters may exist without compromising said separation performance. These values provide meaningful insights into the effect of parameter uncertainty within the context of optimization with constraints on product purity or yield. Such information is essential for hypothetical future applications involving stochastic or robust optimization, where both the nominal parameter values and the nature of their confidence intervals are required. This allows for a more accurate formulation of the problem and a more comprehensive characterization of the system's behavior under uncertainty.

The uncertainty propagation to the predicted model was computed using expression (32). The value obtained for the propagated uncertainty, *Uc*, was 0.0522. This value quantifies the overall uncertainty imposed on the final result by the estimated parameters.

The results shown in Fig. 13 were generated through the execution of 1,000 Monte Carlo simulations.

Considering that the dashed lines shown in Fig. 13 correspond to the dotted and dashed lines presented in Fig. 6, it can be observed that the regions created fully envelop the close-to-optimal model results. It is possible to verify that, depending on the value of the parameters, the model can introduce impurities in the outlet streams, especially in the extract stream. Nonetheless, the uncertainty analysis revealed that the obtained close-to-optimal set of parameters is valid, and that the methodology applied is successful in finding a close-to-optimal fit between simulated and experimental data and the uncertainty in the estimated parameters.

4. Conclusions

In this work, a methodology was developed to estimate parameters, which characterize the equations that describe the separation of BSA and myoglobin in fixed bed and SMB. The methodology consists of creating reference parameters for the fixed bed experiments and obtaining preliminary information about the mechanisms of the separation, which culminates in the estimation of common parameters for fixed bed and SMB.

The parameter estimation for the individual fixed bed experiments, using 100 iterations and 100 particles, yielded a set of reference parameters for each experiment, with close-to-optimal alignment to the experimental data.

The ensuing estimability analysis determined that the mass transfer coefficients, $k_{h,i}$, for both Mb and BSA, do not influence the final model

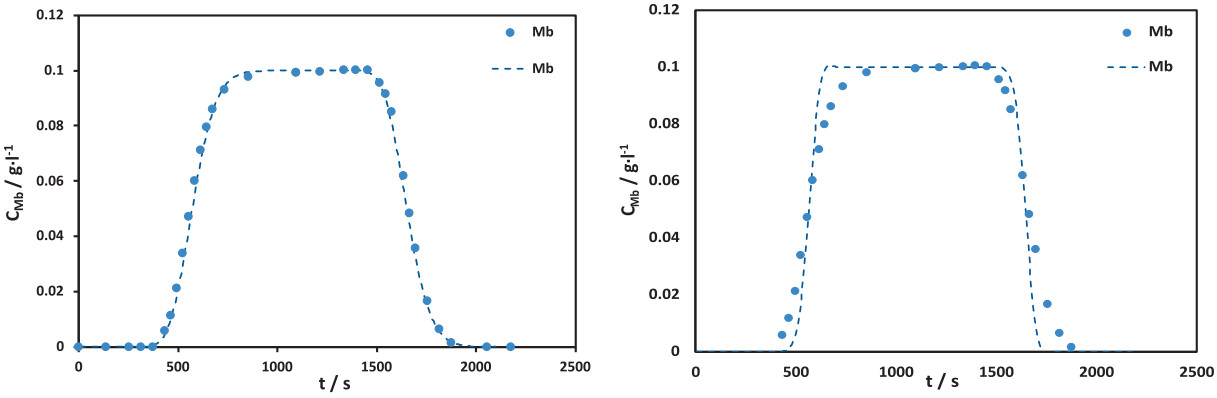

Fig. 8. Graphical comparison between fixed bed reference parameters (left) (R^2 – 0.9956) and estimated parameters yielded by the common parameter estimation (right) (R^2 – 0.9613); experimental data (points); simulated models (dashed lines) – Mb experiment.

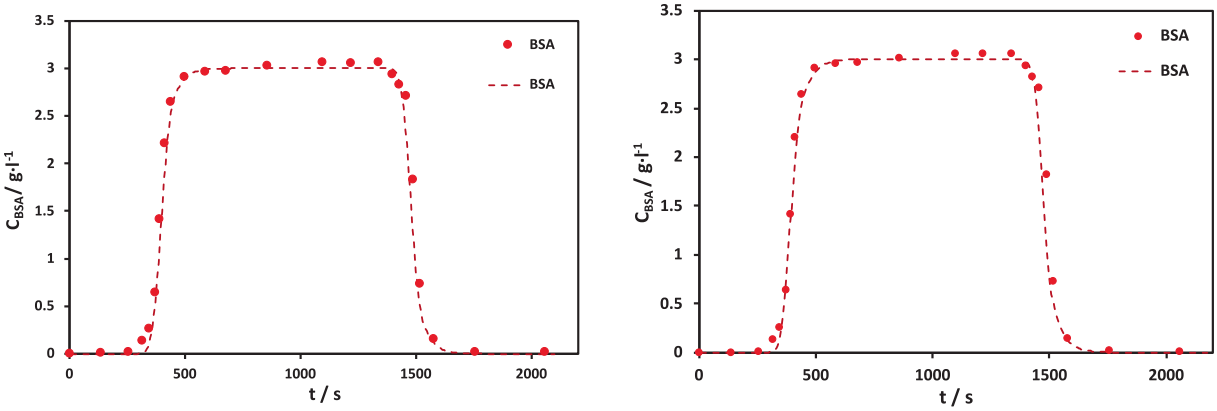

Fig. 9. Graphical comparison between fixed bed reference parameters (left) (R^2 – 0.9402) and estimated parameters yielded by the common parameter estimation (right) (R^2 – 0.9851); experimental data (points); simulated models (dashed lines) – BSA experiment.

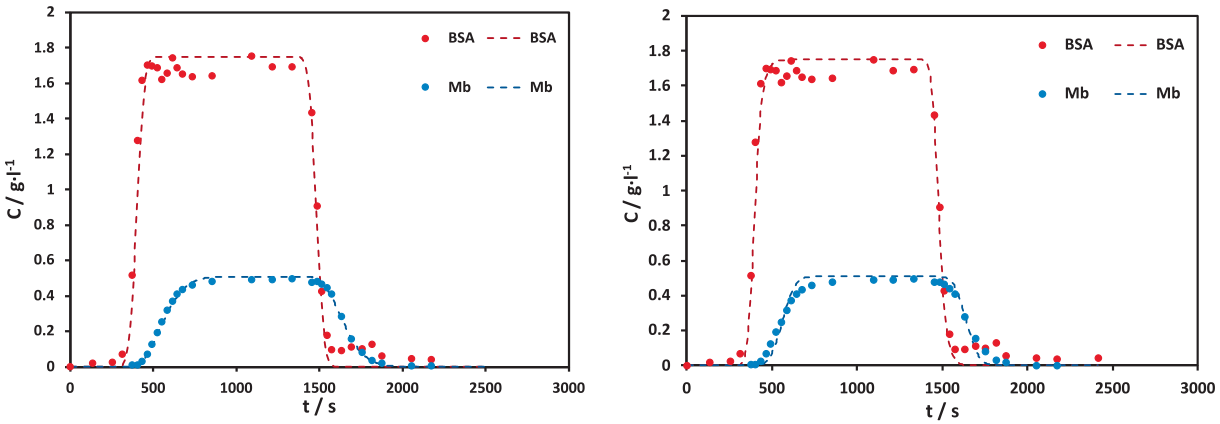

Fig. 10. Graphical comparison between fixed bed reference parameters (left) (R^2 Mb – 0.9956; R^2 BSA – 0.9676) and estimated parameters yielded by the common parameter estimation (right) (R^2 Mb – 0.9858; R^2 BSA – 0.9893); experimental data (points); simulated models (dashed lines) – binary Exp. 1.

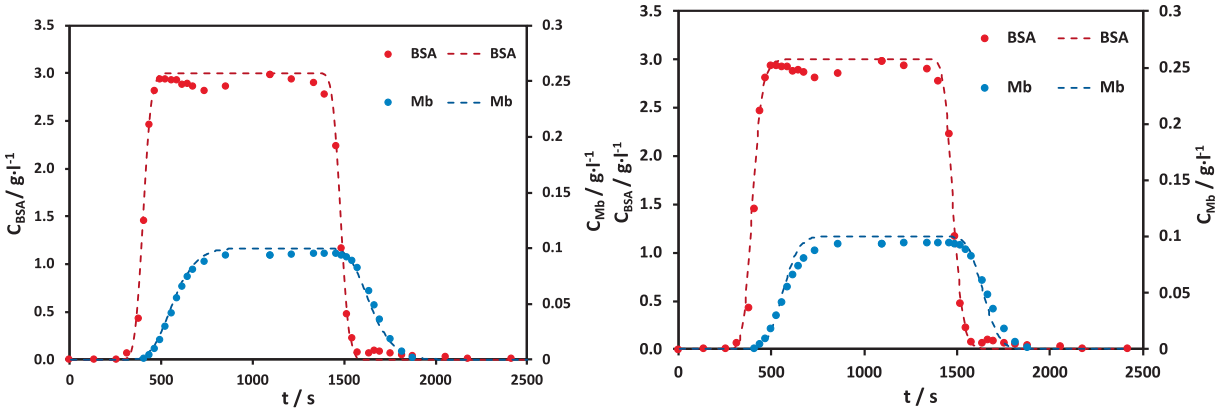

Fig. 11. Graphical comparison between fixed bed reference parameters (left) (R^2 Mb – 0.9922; R^2 BSA – 0.9739) and estimated parameters yielded by the common parameter estimation (right) (R^2 Mb – 0.9802; R^2 BSA – 0.9946); experimental data (points); simulated models (dashed lines) – binary Exp. 2.

Table 13
Objective functions between parameter sets – Mb experiment.

	Rios' Parameters	Reference Parameters	Common Parameters
f_{obj}	1.23 x 10^{-5}	5.01 x 10^{-6}	1.02 x 10^{-4}

Table 14
Objective functions between parameter sets – BSA experiment.

	Rios' Parameters	Reference Parameters	Common Parameters
f_{obj}	0.146	0.0326	0.0362

Table 15
Objective functions between parameter sets – binary experiment.

	Rios' Parameters	Reference Parameters	Common Parameters
f_{obj}	0.0151	0.0107	0.0127

in the chosen parameter boundaries. Therefore, their estimation was considered irrelevant and was removed from further studies.

The parameter estimation using all the experiments available, SMB experiments included, and employing 35 iterations and 50 particles in the PSO, resulted in a set of parameters that created a model with a simultaneous adjustment to the SMB and, overall, to the fixed bed experimental data. Using the reference values obtained during the individual fixed bed studies, it was possible to observe slight differences in some parameters, namely the axial dispersion coefficient, D_{ax}, for the Mb individual experiments and both the axial dispersion coefficient, D_{ax}, and size exclusion constant for BSA, $K_{SEC,BSA}$, in the BSA individual and binary fixed bed experiments. Nonetheless, these variations only negatively affected the model fit to the Mb fixed bed experiment, while the BSA and binary experiments do not reveal significant changes in their respective generated models.

The uncertainty of each of the estimated common parameters was computed to obtain confidence intervals and characterize the results obtained. The propagated uncertainty into the generated model yielded a value of 0.0522.

Some future work can be performed. By applying the methodology to new data generated by the same separation system, it will be possible to further demonstrate the generality, extrapolative capability, and reproducibility of the developed framework. Afterwards, employing this methodology to other stationary phase materials, more complex in nature, is an effective approach to assess the robustness of the methodology. The nature of the system may be changed as well, to explore the robustness even better. A gas-phase separation or the use of other separation equipment may be evaluated using the methodology described here to find possible or eventual limitations and shortcomings.

The methodology considered and used in this work proved to be a successful course of action to estimate parameters in fixed bed and SMB environments and revealed to be a reliable technique to validate the results obtained. Hence, this approach may have the capability of aiding the research studies performed in the domain of parameter estimation for protein purification.

Declaration of generative AI and AI-assisted technologies in the writing process

During the preparation of this work the author(s) used ChatGPT/

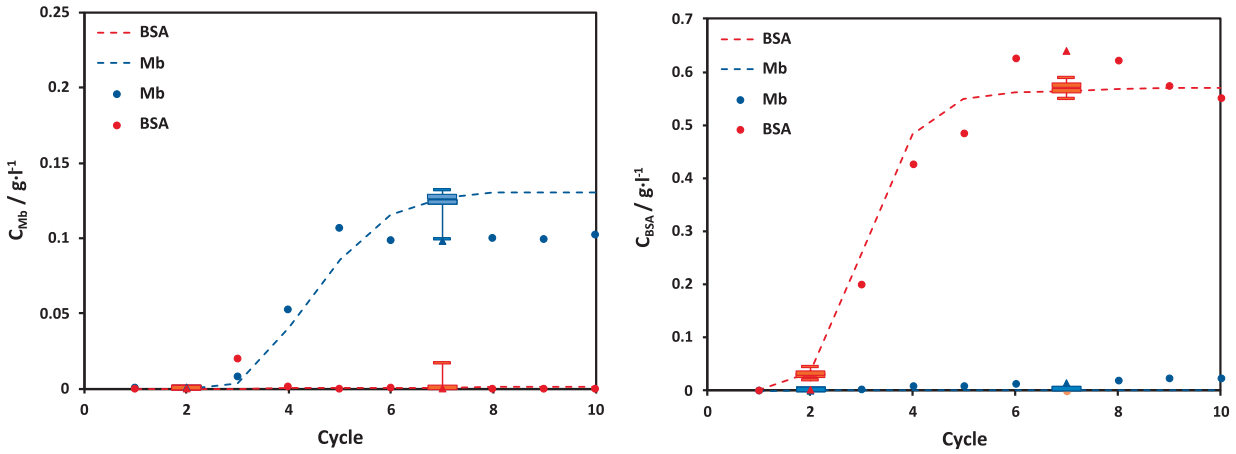

Fig. 12. SMB experimental datasets (dots: training set; triangles: test set) compared with the model obtained from parameter estimation (dashed lines) using the training data. Superimposed boxplot represents quartiles of the model outputs (minimum, first quartile, median, third quartile, and maximum). Extract concentrations are shown on the left, and raffinate concentrations on the right. Note: Boxplots for extract concentrations in cycle 2 overlap.

Table 16
Parameter uncertainties.

Parameter	*Mean value*	*Uncertainty*	*Parameter*	*Mean value*	*Uncertainty*
ε_b	0.3913	± 0.0035	Pe_6	95.764	± 17.945
$D_{ax}(m^2 \bullet s^{-1})$	5.03 x 10^{-8}	± 1.17 x 10^{-7}	$\varepsilon_{b,1}$	0.3897	± 0.0003
$Q_f(m^3 \bullet s^{-1})$	3.24 x 10^{-8}	± 2.76 x 10^{-10}	$\varepsilon_{b,2}$	0.3907	± 0.0003
$K_{SEC,BSA}$	0.040	± 0.018	$\varepsilon_{b,3}$	0.3900	± 0.0005
$K_{SEC,Mb}$	0.319	± 0.091	$\varepsilon_{b,4}$	0.3892	± 0.0003
Pe_1	59.748	± 6.911	$\varepsilon_{b,5}$	0.3909	± 0.0006
Pe_2	80.198	± 9.745	$\varepsilon_{b,6}$	0.3907	± 0.0002
Pe_3	59.082	± 8.637	$Q_F(l \bullet min^{-1})$	8.62 x 10^{-4}	± 1.71 x 10^{-5}
Pe_4	99.608	± 3.390	$Q_D(l \bullet min^{-1})$	5.02 x 10^{-3}	± 1.16 x 10^{-5}
Pe_5	53.520	± 3.973	$Q_X(l \bullet min^{-1})$	3.10 x 10^{-3}	± 9.03 x 10^{-5}
			$Q_{IV}(l \bullet min^{-1})$	1.50 x 10^{-3}	± 5.23 x 10^{-6}

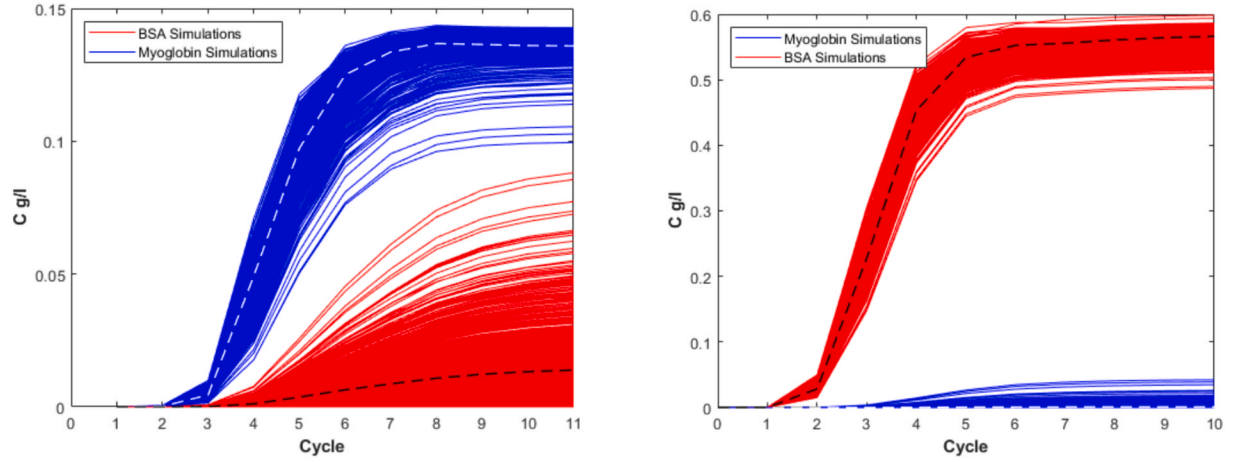

Fig. 13. Monte Carlo simulations pertaining to the extract (left) and raffinate (right) streams. White dashed lines pertain to Myoglobin data while black dashed lines pertain to BSA data, both generated by the model defined by the estimated parameters that yielded the best objective function value.

OpenAI in order to improve the readability and correct eventual grammatical and spelling oversights. After using this tool/service, the author (s) reviewed and edited the content as needed and take(s) full responsibility for the content of the published article.

CRediT authorship contribution statement

Guilherme C. Amaral: Writing – review & editing, Writing – original draft, Visualization, Validation, Software, Methodology, Investigation, Formal analysis, Data curation, Conceptualization. **Albertina G. Rios:** Validation, Resources, Formal analysis, Data curation, Conceptualization. **Alírio E. Rodrigues:** Resources, Project administration, Formal analysis, Data curation, Conceptualization. **Ana M. Ribeiro:** Writing – review & editing, Supervision, Software, Resources, Project administration, Methodology, Investigation, Funding acquisition, Formal analysis, Data curation, Conceptualization. **Diogo Rodrigues:** Writing – review & editing, Visualization, Validation, Software, Methodology, Conceptualization. **Idelfonso B.R. Nogueira:** Writing – review & editing, Visualization, Supervision, Visualization, Software, Resources, Project administration, Methodology, Investigation, Funding acquisition, Formal analysis, Data curation, Conceptualization. **Alexandre F.P. Ferreira:** Writing – review & editing, Visualization, Supervision, Visualization, Software, Resources, Project administration, Methodology, Investigation, Funding acquisition, Formal analysis, Data curation, Conceptualization.

Declaration of competing interest

The authors declare that they have no known competing financial interests or personal relationships that could have appeared to influence the work reported in this paper.

Acknowledgements

This research was supported by Fundação para a Ciência e a Tecnologia, I.P. /MCTES through national funds: LSRE-LCM, UID/50020/2025 (DOI: 10.54499/UID/50020/2025); and ALiCE, LA/P/0045/2020 (DOI: 10.54499/LA/P/0045/2020).

Data availability

Data will be made available on request.

References

Whitford, D., 2013. Proteins: Structure and Function. John Wiley & Sons.
Kumar, M., et al., 2022. Plant-based proteins and their multifaceted industrial applications. LWT 154, 112620. https://doi.org/10.1016/j.lwt.2021.112620, 2022/01/15/.
Hey, T., Fiedler, E., Rudolph, R., Fiedler, M., 2005. Artificial, non-antibody binding proteins for pharmaceutical and industrial applications. Trends Biotechnol. 23 (10), 514–522. https://doi.org/10.1016/j.tibtech.2005.07.007, 2005/10/01/.
Ryu, H., et al., 2019. Biomimetic membranes with transmembrane proteins: state-of-the-art in transmembrane protein applications,“ 20(6), p. 1437, [Online]. Available: https://www.mdpi.com/1422-0067/20/6/1437.
Nfor, B.K., et al., 2008. Design strategies for integrated protein purification processes: challenges, progress and outlook 83 (2), 124–132. https://doi.org/10.1002/jctb.1815.
Smith, D.M., 2017. Protein separation and characterization procedures. In: Food Analysis, S. S. Nielsen Ed. Cham: Springer International Publishing, pp. 431-453.
Saxena, A., Tripathi, B.P., Kumar, M., Shahi, V.K., 2009. Membrane-based techniques for the separation and purification of proteins: an overview. Adv. Colloid Interface Sci. 145 (1), 1–22. https://doi.org/10.1016/j.cis.2008.07.004, 2009/01/30/.
Liu, S., Li, Z., Yu, B., Wang, S., Shen, Y., Cong, H., 2020. Recent advances on protein separation and purification methods. Adv. Colloid Interface Sci., 284, p. 102254, 2020/10/01/, doi: https://doi.org/10.1016/j.cis.2020.102254.
Lundanes, E., Reubsaet, L., Greibrokk, T., 2013. Chromatography: basic principles, sample preparations and related methods. John Wiley & Sons.
Hunt, B.J., Holding, S.R., 2013. Size exclusion chromatography. Springer Science & Business Media.
Houwing, J., 2003. Separation of proteins by simulated moving bed chromatography.
Rodrigues, A., 2015. Simulated moving bed technology: principles, design and process applications. Butterworth-Heinemann.
Xu, Z., Cai, J.-G., Pan, B.-C., 2013. Mathematically modeling fixed-bed adsorption in aqueous systems. J. Zhejiang Univ. Sci. A 14 (3), 155–176. https://doi.org/10.1631/jzus.A1300029, 2013/03/01.
Pinto, J.C., Schwaab, M., 2007. Análise de Dados Experimentais: I. Fundamentos de Estatística e Estimação de Parâmetros, Editora E-papers.
Lin, M.-H., Tsai, J.-F., Yu, C.-S., 2012. A review of deterministic optimization methods in engineering and management. Math. Probl. Eng. 2012, 756023. https://doi.org/10.1155/2012/756023, 2012/06/20.
Martí, R., Reinelt, G., 2022. Heuristic methods,“ in Exact and Heuristic Methods in Combinatorial Optimization: A Study on the Linear Ordering and the Maximum Diversity Problem, R. Martí and G. Reinelt Eds. Berlin, Heidelberg: Springer Berlin Heidelberg, pp. 27-57.
Rao, S.S., 2019. Engineering optimization: theory and practice. John Wiley & Sons.
Coelho, L.D.S., Sierakowski, C.A., 2008. A software tool for teaching of particle swarm optimization fundamentals. Adv. Eng. Softw. 39 (11), 877–887. https://doi.org/10.1016/j.advengsoft.2008.01.005, 2008/11/01/.
Schwaab, M., 2005. “Evaluation of heuristic optimization algorithms in parameter estimation problems,” UFRJ.
Kennedy, J., Eberhart, R., 1995. “Particle swarm optimization,” in Proceedings of ICNN'95 - International Conference on Neural Networks, 27 Nov.-1 Dec. 1995, vol. 4, pp. 1942-1948 vol.4, doi: 10.1109/ICNN.1995.488968.
Yao, K.Z., Shaw, B.M., Kou, B., McAuley, K.B., Bacon, D.W., 2003. Modeling ethylene/butene copolymerization with multi-site catalysts: parameter estimability and experimental design. Polym. React. Eng. 11 (3), 563–588. https://doi.org/10.1081/PRE-120024426, 2003/01/09.
Nogueira, I.B.R., Ribeiro, A.M., Rodrigues, A.E., Loureiro, J.M., 2016. Dynamics of a true moving bed separation process: effect of operating variables on performance indicators using orthogonalization method. Comput. Chem. Eng. 86, 5–17. https://doi.org/10.1016/j.compchemeng.2015.12.009, 2016/03/04/.
Nogueira, I.B.R., Pontes, K.V., 2017. Parameter estimation with estimability analysis applied to an industrial scale polymerization process. Comput. Chem. Eng. 96, 75–86. https://doi.org/10.1016/j.compchemeng.2016.10.013, 2017/01/04/.
I. Iso and B. J. G. OIML, Switzerland, “Guide to the Expression of Uncertainty in Measurement,” vol. 122, pp. 16-17, 1995.
Kroese, D.P., Brereton, T., Taimre, T., Botev, Z.I., 2014. Why the monte carlo method is so important today. WIREs Comput. Stat. 6 (6), 386–392. https://doi.org/10.1002/wics.1314.
Crowe, C.M., 1996. Data reconciliation — Progress and challenges. J. Process Control 6 (2), 89–98. https://doi.org/10.1016/0959-1524(96)00012-1, 1996/04/01/.
Santos, R.V.A., et al., 2021. Global approach for simulated moving bed model identification: design of experiments, uncertainty evaluation, and optimization strategy assessment. Ind. Eng. Chem. Res. 60 (21), 7904–7916. https://doi.org/10.1021/acs.iecr.1c01276, 2021/06/02.
Schwaab, M., Biscaia, J.E.C., Monteiro, J.L., Pinto, J.C., 2008. Nonlinear parameter estimation through particle swarm optimization. Chem. Eng. Sci. 63 (6), 1542–1552. https://doi.org/10.1016/j.ces.2007.11.024, 2008/03/01/.
He, Q., Wang, L., Liu, B., 2007. Parameter estimation for chaotic systems by particle swarm optimization, 2007/10/01/ Chaos, Solitons Fractals 34 (2), 654–661. https://doi.org/10.1016/j.chaos.2006.03.079.
Gill, M.K., Kaheil, Y.H., Khalil, A., McKee, M., Bastidas, L., 2006. “Multiobjective particle swarm optimization for parameter estimation in hydrology,” 42(7), doi: https://doi.org/10.1029/2005WR004528.
Ouyang, A., Li, K., Truong, T.K., Sallam, A., Sha, E.H.M., 2014. Hybrid particle swarm optimization for parameter estimation of Muskingum model. Neural Comput. & Applic. 25 (7), 1785–1799. https://doi.org/10.1007/s00521-014-1669-y, 2014/12/01.
Sakthivel, V.P., Bhuvaneswari, R., Subramanian, S., 2010. Multi-objective parameter estimation of induction motor using particle swarm optimization. Eng. Appl. Artif. Intel. 23 (3), 302–312. https://doi.org/10.1016/j.engappai.2009.06.004, 2010/04/01/.
Grosfils, V., Hanus, R., Wouwer, A.V., Kinnaert, M., 2010. Parametric uncertainties and influence of the dead volume representation in modelling simulated moving bed separation processes. J. Chromatogr. A 1217 (47), 7359–7371. https://doi.org/10.1016/j.chroma.2010.09.030, 2010/11/19/.
Grosfils, V., Levrie, C., Kinnaert, M., Vande Wouwer, A., 2007. A systematic approach to SMB processes model identification from batch experiments. Chem. Eng. Sci. 62 (15), 3894–3908. https://doi.org/10.1016/j.ces.2007.04.015, 2007/08/01/.
Bentley, J., Sloan, C., Kawajiri, Y., 2013. Simultaneous modeling and optimization of nonlinear simulated moving bed chromatography by the prediction–correction method. J. Chromatogr. A 1280, 51–63. https://doi.org/10.1016/j.chroma.2013.01.026, 2013/03/08/.
Kawajiri, Y., Biegler, L.T., 2008. Comparison of configurations of a four-column simulated moving bed process by multi-objective optimization. Adsorption 14 (2), 433–442. https://doi.org/10.1007/s10450-007-9074-9, 2008/06/01.
Suzuki, K., et al., 2022. Utilization of operation data for parameter estimation of simulated moving bed chromatography 4 (1), e10103. https://doi.org/10.1002/amp2.10103.
Chen, J., Chen, M., Chan, L.L.T., 2010. Iterative learning parameter estimation and design of SMB processes. Chem. Eng. J. 161 (1), 223–233. https://doi.org/10.1016/j.cej.2010.04.027, 2010/07/01/.
He, Q.-L., von Lieres, E., Sun, Z., Zhao, L., 2020. Model-based process design of a ternary protein separation using multi-step gradient ion-exchange SMB chromatography. Comput. Chem. Eng. 138, 106851. https://doi.org/10.1016/j.compchemeng.2020.106851, 2020/07/12/.

Rios, A.G., Ribeiro, A.M., Rodrigues, A.E., Ferreira, A.F.P., 2020. Bovine serum albumin and myoglobin separation by size exclusion SMB. J. Chromatogr. A 1628, 461431. https://doi.org/10.1016/j.chroma.2020.461431, 2020/09/27/.

Hendgen-Cotta, U.B., Kelm, M., Rassaf, T., 2014. Myoglobin functions in the heart. Free Radic. Biol. Med. 73, 252–259. https://doi.org/10.1016/j.freeradbiomed.2014.05.005, 2014/08/01/.

Essa, H., Magner, E., Cooney, J., Hodnett, B.K., 2007. Influence of pH and ionic strength on the adsorption, leaching and activity of myoglobin immobilized onto ordered mesoporous silicates. J. Mol. Catal. B Enzym. 49 (1), 61–68. https://doi.org/10.1016/j.molcatb.2007.07.005, 2007/11/16/.

Peters, T., 1970. "Serum Albumin," in Advances in Clinical Chemistry, vol. 13, O. Bodansky and C. P. Stewart Eds.: Elsevier, pp. 37-111.

Peters Jr, T., 1995. All about albumin: biochemistry, genetics, and medical applications. Academic Press.

Rios, A.G., Ribeiro, A.M., Rodrigues, A.E., Quadros, P.A., Ferreira, A.F.P., 2023. Bovine serum albumin and myoglobin separation on HAp. Sep. Purif. Technol. 326, 124779. https://doi.org/10.1016/j.seppur.2023.124779, 2023/12/01/.

Rios, A.G., Ribeiro, A.M., Rodrigues, A.E., Ferreira, A.F.P., 2023. Bovine serum albumin and myoglobin separation by ion-exchange SMB. Ind. Eng. Chem. Res. 62 (35), 13932–13942. https://doi.org/10.1021/acs.iecr.3c01613, 2023/09/06.

Kravaris, C., Hahn, J., Chu, Y.J.C., and c. engineering, 2013. Advances and selected recent developments in state and parameter estimation, vol. 51, pp. 111-123.

Rebello, C.M., Martins, M.A.F., Loureiro, J.M., Rodrigues, A.E., Ribeiro, A.M., Nogueira, I.B.R., 2021. From an optimal point to an optimal region: a novel methodology for optimization of multimodal constrained problems and a novel constrained sliding particle swarm optimization strategy. Mathematics, 9(15), p. 1808, [Online]. Available: https://www.mdpi.com/2227-7390/9/15/1808.

Benyahia, B., Latifi, M.A., Fonteix, C., Pla, F., 2013. Emulsion copolymerization of styrene and butyl acrylate in the presence of a chain transfer agent. Part 2: Parameters estimability and confidence regions. Chem. Eng. Sci. 90, 110–118. https://doi.org/10.1016/j.ces.2012.12.013, 2013/03/07/.